

# International Conference on Space Optics—ICSO 2022

Dubrovnik, Croatia

3–7 October 2022

*Edited by Kyriaki Minoglou, Nikos Karafolas, and Bruno Cugny,*



***Manufacturing of a highly efficient gold coated echelle grating for NIR on a thick silicon substrate with small straylight and wavefront error***



# Manufacturing of a highly efficient gold coated echelle grating for NIR on a thick silicon substrate with small straylight and wavefront error

Susann Sadlowski<sup>\*a</sup>, Thomas Flügel-Paul<sup>a</sup>, François Wildi<sup>b</sup>, Martin Wittig<sup>a</sup>, Tino Benkenstein<sup>a</sup>, Jan Nathanael<sup>a</sup>, Marcus Trost<sup>a</sup>, Peter Munzert<sup>a</sup>, Michael Scheler<sup>a</sup>, Uwe D. Zeitner<sup>a</sup>

<sup>a</sup>Fraunhofer Institute for Applied Optics and Precision Engineering IOF, Albert-Einstein-Straße 7, 07745 Jena, Germany; <sup>b</sup>Department of Astronomy, University of Geneva, Chemin Pegasi 51, 1290 Sauverny, Switzerland

## ABSTRACT

We present the design, manufacturing and characterization results of a customized high-resolution echelle grating. The grating was manufactured at Fraunhofer IOF and delivered to the NIRPS (Near Infrared Planet Searcher Instrument) consortium. The technology workflow for the manufacturing of the echelle grating is relying on wet-chemical etching, applied to crystalline silicon substrates, which enables the creation of highly determined micro-facets and surfaces over macroscopic dimensions. The echelle's grating period and plateau size within one period are established based on electron-beam lithography. A binary pattern in a hard mask material is performed by dry-reactive ion etching while transferring the pattern in the silicon substrate is achieved by wet-chemical etching with potassium hydroxide.

The grating is designed to operate at a blaze angle of  $76^\circ$  in a wavelength band of  $0.9\mu\text{m} - 1.8\mu\text{m}$ . A gold coating is applied to increase the diffraction efficiency to about 70%; verified at wavelengths of 1030nm and 1640nm, respectively. The overall grating size is 78mm x 284mm providing a WFE of less than 70nm (RMS) measured throughout the full aperture. In this article we present the manufacturing workflow and structural inspection results of the manufactured echelle grating, having a critical eye on the impact of sub-surface defects of the initial silicon crystal. Moreover, we present optical performance test results covering diffraction efficiency, PSF, WFE and spectral ghosts. It is concluded that the imaging properties of the manufactured grating are as good as those of a plane gold mirror reference.

**Keywords:** echelle grating, reflection grating, infrared optics, low aberration, electron-beam lithography

## 1. INTRODUCTION

Within the last decade the search for exoplanets gained increasing interest within the scientific community. Optical and near-infrared spectroscopy is nowadays the method of choice to search and characterize exoplanets even at huge astronomical distances.

Among others, a consortium based around the Institute for Research on Exoplanets (iREx) from the University of Montreal and the department of Astronomy from the University of Geneva is currently deploying NIRPS, a Doppler spectrograph for M-dwarf monitoring and low-mass exoplanet characterization [1].

Common echelle gratings are typically manufactured using ruling technologies, i.e. material is ablated via specialized mechanical tooling from the initial substrate surface. Ruling technology is limited to the usage of sufficiently soft materials (e.g. gold). The scaling to echelle grating structures with feature sizes in the order of  $100\mu\text{m}$  is not trivial. Removing a large amount of material typically leads to imperfections in the micro-structured profile which again might decrease the optical performance.

The design parameters for the high-performance near infrared spectrometer present an unprecedented challenge. The limiting issue is to manufacture a state-of-the-art echelle-type grating on a monolithic 15mm thick silicon substrate with wavefront error smaller than 158nm (RMS) on a full 78mm x 284mm grating area. Table 1 summarizes the most important performance specifications of the echelle grating provided by the NIRPS consortium.

\*susann.sadlowski@iof.fraunhofer.de; phone +49 3641 807450; <http://www.iof.fraunhofer.de>

## 1.1 Requirements

Table 1. NIRPS grating requirements.

Parameter	Value
substrate material	silicon
grating type	blazed grating
wavelength range	0.9 $\mu\text{m}$ – 1.8 $\mu\text{m}$
reference wavelength	1.5 $\mu\text{m}$
clear aperture element size	74mm x 280mm 90mm x 292mm
substrate thickness	15mm
grating period	75 $\mu\text{m}$
blaze angle	76° +/- 0.5°
plateau area	< 9% (goal < 7%)
reflection coating	gold
grating diffraction efficiency	> 60% (goal: > 70%)
ghost efficiency	< 10 <sup>-3</sup> (goal: < 10 <sup>-4</sup> )
wavefront error	WFE < 158nm RMS (goal: < 63nm RMS)

## 2. ECHELLE GRATING MANUFACTURING

### 2.1 Echelle design

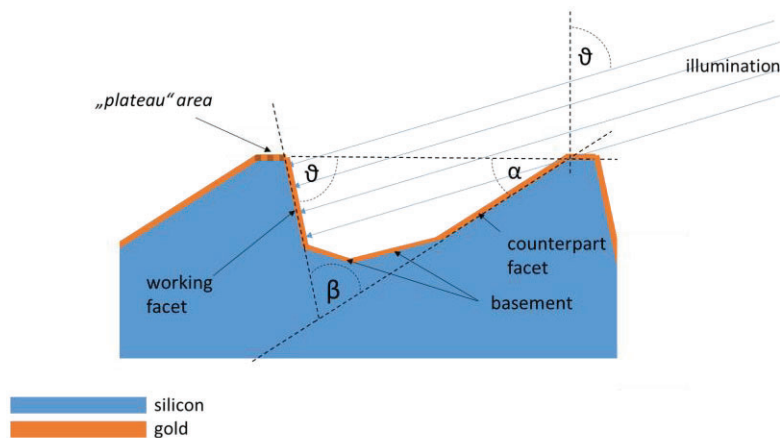


Figure 1. Sketch of the grating geometry.

In Figure 1 the grating geometry is sketched. The angle  $\vartheta$  is the blaze angle. The angle  $\beta$  is defined by the crystallographic structure of silicon (being the intersection angle between two different (111)-crystallographic planes) and amounts to  $70.53^\circ$ . The plateau area is a consequence of the lithographic manufacturing process and cannot be avoided in general. Typical widths are 3% - 9% of the period of the grating. The correct blaze angle is entirely determined by the crystallographic orientation and not by the lithography process. During substrate preparation, i.e. sawing of the actual substrate out of its ingot, the blaze angle can be typically controlled with a precision of  $\pm 0.2^\circ$  and its actual value is certified by the substrate supplier.

The etching process was performed in several iterations interrupted by subsequent SEM inspections to analyze and control the proper evolution of the evolving micro-facets. Finally, the etching process was stopped at a final depth of the “working facet” of  $\sim 25\mu\text{m}$  (determined perpendicular to the unstructured surface) which guarantees a safety margin of  $\sim 7\mu\text{m}$  before shadowing effects will reduce achievable diffraction efficiency. In consequence, a residual “basement” with a certain width is remaining between the two major facets, i.e. “working facet” and “counterpart facet”, that are determined in (111) crystallographic directions and being highly stable with respect to the applied wet-etching process.

## 2.2 Manufacturing workflow

A brief sketch of the manufacturing workflow is depicted in the following Figure 2. The manufacturing of the NIRPS grating starts with the cleaning and coating of the silicon substrate. Here, chromium is sputtered as a hard mask material. Afterwards, the resist is applied for the lithography process. The binary mask is exposed via electron beam lithography. A first patterning of the chromium mask is realized with dry reactive ion etching. Between the exposure and various patterning steps, the structure feature sizes are controlled and verified with Scanning Electron Microscopy (SEM). The chromium pattern is transferred into the silicon substrate material via wet chemical etching and with a tailored in-house developed setup to enable to process such large and customized substrates. The wet-chemical etching is performed with potassium hydroxide. The etching process is highly anisotropic such that the final shape of the grating structure is determined by those planes of the silicon crystal which exhibit the lowest etching rates, i.e. all planes of (111) family. After the wet chemical etching process the mask material is removed. A final SEM investigation after cleaning the grating from organic residuals with peroxymonosulfuric acid (or: Caro’s acid) is performed. The gold layer is applied via evaporation.

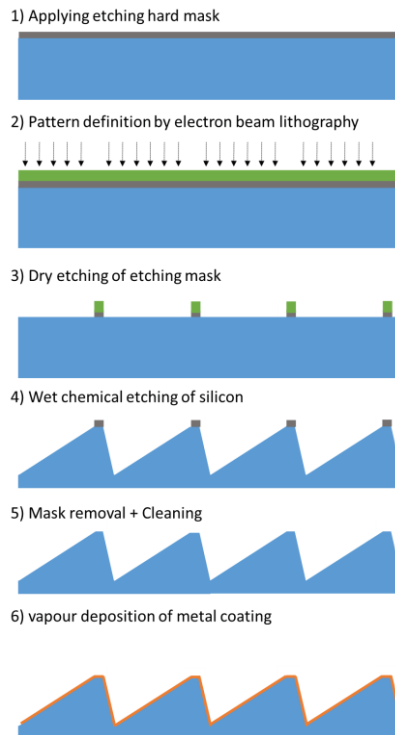


Figure 2. Grating technology workflow.

The basis for a successful grating manufacturing is the substrate blank and its properties. The substrate consists of crystalline silicon with a customized crystallographic orientation, i.e. Si <100> tilted by  $21.26^\circ \pm 0.1^\circ$  with respect to the surface normal of the substrate. The following equation provides the relation between tilt angle and required blaze angle of the echelle grating:

$$\text{blaze angle} = \arccos \sqrt{1/3} + \text{tilt angle} = 54.74^\circ + 21.26^\circ = 76.0^\circ \pm 0.1^\circ \quad (1)$$

For achieving the required substrate quality we worked with a high precision polished silicon substrate, manufactured by Carl Zeiss SMT GmbH. It has an ultra-low surface height error of 17nm RMS and a surface roughness of < 0.5nm RMS over a clear aperture (CA) of 280mm x 130mm, see Table 2 and Figure 3.

Table 2. Initial substrate properties verified by Zeiss SMT.

Property (Zeiss)	Result
surface height error	17nm RMS
surface roughness	< 0.5nm RMS

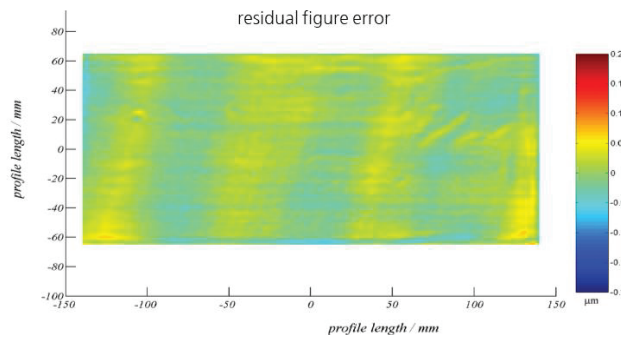


Figure 3. Measured geometry / surface error at Carl Zeiss SMT GmbH.

### 2.3 Mechanical Dimensions and Clear Aperture Dimensions

The substrate has a rectangular geometry of 292mm x 150mm x 15mm. The grating area has a CA of 74mm x 280mm on the one, ultra- precise polished surface. Figure 4 shows the incoming inspection of this high precision manufactured blank substrate at IOF. Critically important to note, essentially no cosmetic surface defects or contaminations like scratches or digs were observed. The substrate's outer surface preparation appears to be *perfect*.



Figure 4. Silicon substrate at visual incoming inspection before start of grating manufacturing.

### 3. MANUFACTURING RESULTS

The final manufactured microstructure grating geometry is shown in Figure 5. It is the top view of the grating after removing the mask material and the cleaning of organic residuals. The relevant lateral feature sizes are measured i.e. the plateau width, grating period, working facet and the counterpart facet. The grating period is verified at a single location and was determined via SEM. It amounts to  $74.92\mu\text{m}$ . Considering the limited accuracy of this measurement method a period of  $75\mu\text{m}$  can be confirmed. Assuming a blaze angle of  $76^\circ \pm 0.5^\circ$  we calculate with a measured, projected working facet's lateral width of  $7.146\mu\text{m}$ . With this feature size and the knowledge of the angular relations of  $\tan 76^\circ = \text{working facet} / 7.146\mu\text{m}$  we calculate a  $28.7\mu\text{m} \pm 1\mu\text{m}$  depth of the working facet. Therefore, the necessary target depth of  $\sim 25\mu\text{m}$  was achieved with more than  $7\mu\text{m}$  safety margin. Hence, optical shadowing effects are considered to not occur such that diffraction efficiency will not be negatively impacted. Moreover, the plateau area width is determined to be  $4.8\mu\text{m}$  corresponding to a ratio of 6.4% of the grating's period, thus, slightly beating the goal requirement of  $< 7\%$  (see Table 1).

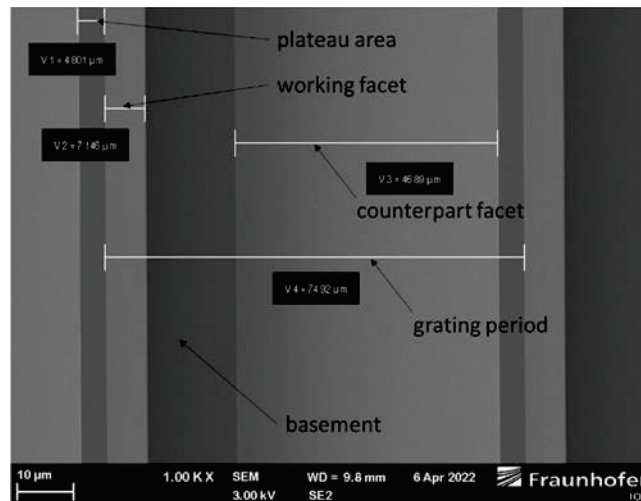


Figure 5. SEM specified groove density of the silicon grating.

A further reduction of the plateau width would increase the gratings diffraction efficiency, however, at the cost of higher risk of so-called breakthroughs of the etching under the hard mask mainly triggered at material defects or crystallographic imperfections. An example of imperfect micro-facets is provided in Figure 6.

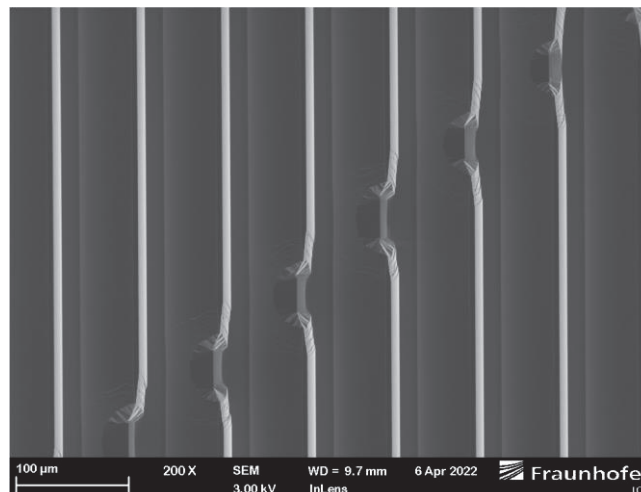


Figure 6. SEM of silicon grating area with SSDs.

A thorough analysis of several such imperfections reveals the following aspects: i) Defects are a local imperfection of the silicon crystallographic structure, especially those of the (111)-planes. Such sites are thus not sufficiently resistant against etching with potassium hydroxide. ii) On the macro-scale, such defects do mainly manifest in elongated lines or curves becoming more and more prominent the longer the wet-etching process is performed (see Figure 7). In particular, they are not observable prior to the initial start of the wet-etching process (see Section 2.3 for comparison). iii) Defect lines that are observable by eye on the macro-scale are constituted by a discrete set of densely arranging point-like defects where the etching process was not properly confined by the chromium mask resulting in local "breakthroughs" underneath the mask pattern.

In conclusion, the defect lines that are slowly evolving during the etching of the micro-facets are the consequence of so-called sub surface damages (SSDs) – damages of the monocrystalline structure of the silicon which have a negative impact on the wet etching process.



Figure 7. Final visual inspection of the gold coated NIRPS grating before delivery.

SSDs of crystalline silicon are known to be introduced by surface preparation processes as for example grinding, lapping and polishing. Such processes are known to induce high mechanical loads and stresses inside the material, which leads to the sub surface damages. Essentially, dislocations, microcracks, stacking faults and other defects to the crystal structure might be introduced [2][3][4][5].

A further process optimization aiming at avoiding SSDs (thus reducing defects at the final grating surface) was not performed. However, such process optimization must focus on the substrate preparation processes (grinding and polishing). Eventually, it is the delicate task to find a suitable balance or trade-off between – on the one hand - a low density of SSDs and – on the other hand – low surface shape errors. Avoiding SSDs typically requires applying soft polishing tools like chemo-mechanical polishing (CMP) whereas high surface planarity (and thus low WFE) rather requires robust polishing tools and processes like pitch polishing.

## 4. OPTICAL MEASUREMENTS

### 4.1 Diffraction Efficiency

The diffraction efficiency measurement is one of the central and most important verification methods for the NIRPS grating. It was measured with a tunable diode laser at the wavelengths 1033nm and 1640nm independently in TE and TM polarization. The spot size is smaller than 2mm and it is laterally scanned with a 2mm pitch over an area of ~220mm x 78mm. The angle of incidence (AOI) is 75.5°.

By intention, the AOI is chosen to be close to *but not exactly matching* the Littrow condition ensuring a proper separation of the diffracted orders from the incident beam. For this reason, the diffraction efficiency is determined by adding the measurement values of those two diffraction orders that are closest in diffraction angle to the incident beam. We call it the “low” and “high” diffraction order, indicating that one of the two orders has a diffraction angle slightly lower (or higher) than the AOI. However, numerical modelling of the grating’s microstructure reveals that the true diffraction efficiency (peak value in true Littrow condition) is roughly 2% lower than the sum of “low” and “high” order. In the following Figure 8 the polarization averaged efficiencies for both wavelengths are depicted. Based on limitations in the measurement setup the full measuring size is restricted to 78mm x ~225mm.

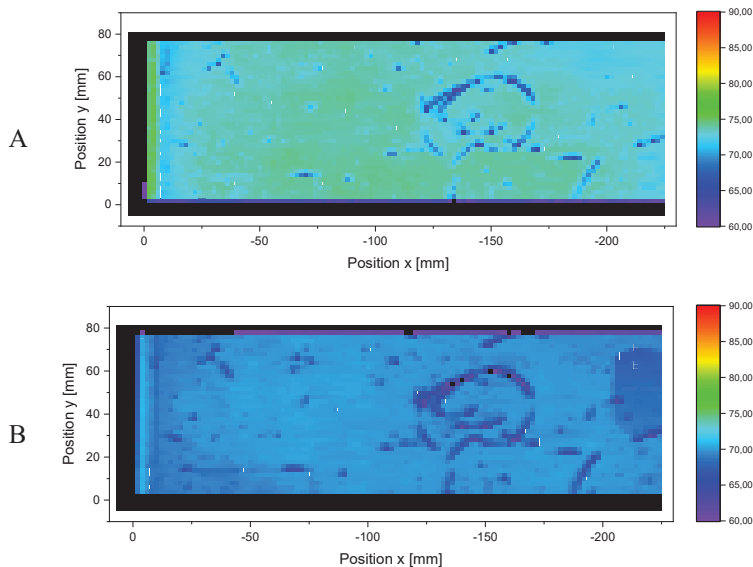


Figure 8. Polarization averaged diffraction efficiency in percent, measured at wavelengths A:1033nm and B: 1640nm.

The measurements show the dependency of the diffraction efficiency with respect to the lateral position within the grating aperture. Impacts of surface imperfections caused by SSDs (see Section 3) can be clearly monitored. Nevertheless, the mean diffraction efficiency amounts at 1033nm (A) to  $73\% \pm 1\%$  and at 1640nm (B) to  $69\% \pm 1\%$ . In consequence, the target requirement of  $> 60\%$  (see Table 1) is well exceeded.

#### 4.2 Imaging quality

The imaging quality of the diffraction grating is a parameter that is indirectly very important because the image size will limit the spectral resolution and the image quality is taken into account in the computation of the efficiency.

To assess the image quality of the grating the University of Geneva has made a direct measurement of the PSF with a monomode fiber. Because the bench is large and has no cover, maintaining diffraction limited performance despite ventilation in the clean room and temperature variations has been a challenge. To single out the performance of the grating (and not measure the performance of the full bench) alternate measurements with the grating are performed as well as with a reference plane mirror. The optical parameters of the grating are measured on a bench made of:

- A source/detector unit where the source is either a 200mm multi-mode fiber or a SMA28 monomode fiber and the detector is a 320 x 256 InGaAs infrared detector. Source and detector center are optically conjugated through a beam-splitter
- An  $\lambda/8$  off-axis parabola producing a collimated beam illuminating the full grating aperture.

The grating itself is mounted on an indexed turn table. The optical setup is shown in Figure 9.

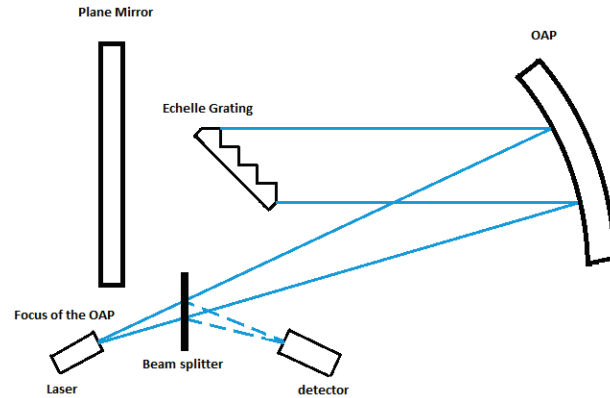


Figure 9. Setup used for the optical characterization of the grating at the University of Geneva.

Figure 10 below shows that there is no significant difference between the FWHM of the grating PSF and the PSF taken with the reference mirror. Therefore, we claim that the grating is fully diffraction limited giving a full aperture resolution of roughly  $400''000$ .

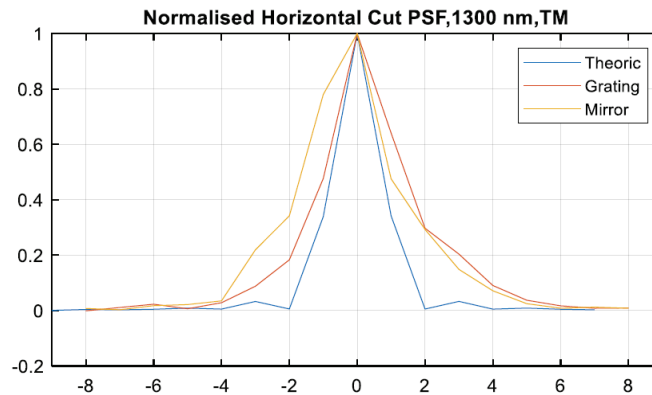


Figure 10. Full aperture image quality at 1300nm.

### 4.3 Reflected Wavefront Error

One further requirement analysis of the final NIRPS grating is the measurement of the reflected wavefront error (rWFE). For comparison: the initial substrate blank had a surface height error of 17nm RMS (see Section 0). Through the influences of the micro-structuring process and the gold coating process it was requested to reach a goal WFE  $< \lambda/10$  at 632.8nm. The interferometric measurement setup is shown in Figure 11 and the resulting WFE is given in Figure 12.

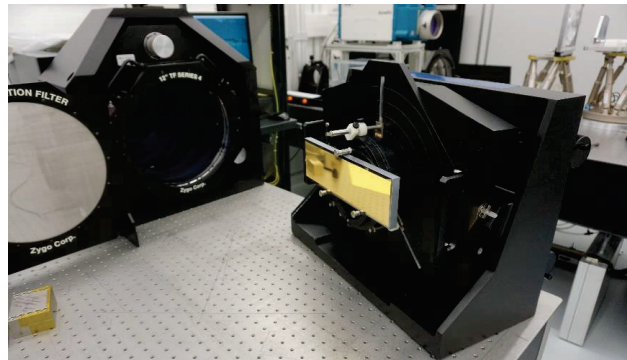


Figure 11. Measurement setup of Interferometry measurement.

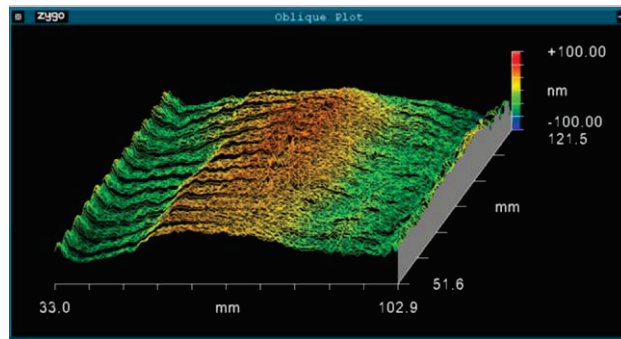


Figure 12. Result of reflected WFE.

There, we measured at 632.8nm wavelength and an AOI of  $75.5^\circ \pm 0.5^\circ$  (see Figure 12) with circular polarization under retro-reflection. The measured WFE was analyzed within an aperture of 70mm. Piston and tilt are removed. The residual WFE of the reflected beam is 248nm (PV) or 54nm (RMS), respectively.

#### 4.4 Spectral Ghosts

To investigate the spectral ghosts, we have over-exposed the sensor by a factor of about 3400 and we have scanned the grating in rotation from the brightest order to the next, looking for spurious signals in-between. We have not been able to identify ghost above 0.03 relative to the level of the detector saturation. Therefore, we estimate that no ghost above a relative level of  $0.03/3400 \cong 10^{-5}$  is present in the spectrum.

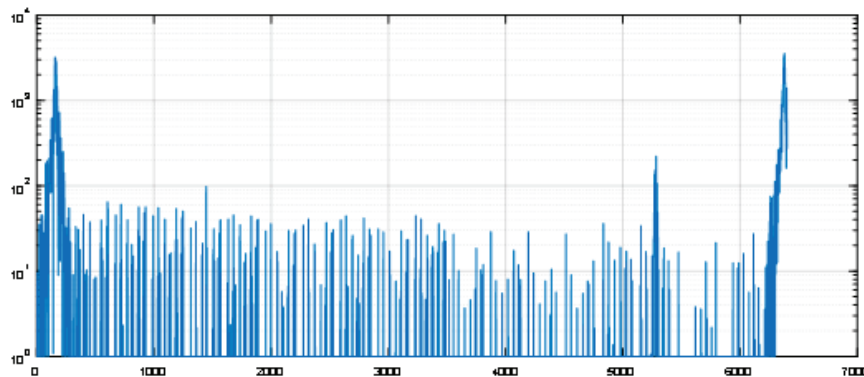


Figure 13. Horizontal scan between 2 diffraction orders at 1300nm. The diffraction orders at the ends of the scan are saturated by a factor of 3400. The “spurious” peak on the right side is an interference in the beam splitter between source and detector. It does not move when the grating is rotated.

## 5. CONCLUSION

We have successfully manufactured and characterized a gold-coated, large silicon echelle grating for the NIRPS mission. The new technology process relies on crystalline silicon which is wet-chemically etched to establish the micro-facets of the echelle grating. The preparation of the silicon substrate turned out to be the most critical and delicate process within the entire manufacturing chain. Despite substantial effort which was spend during project runtime, we did not succeed in finding a proper balance between minimizing surface shape error on the one side and completely avoiding sub-surface damages on the other side. Eventually, the density of SSDs (manifesting in e.g. defect lines and high-density point defects) could be reduced, nevertheless, they still cannot be exterminated entirely. However, the pure optical performance is not impacted by sub-surface damages as proven by verification measurements. The grating exhibits an outstanding performance with respect to:

- diffraction efficiency being close to the theoretical limit

- the point-spread function being comparable with that of a plane mirror
- spectral ghosts with relative efficiencies smaller than  $10^{-5}$ .

## REFERENCES

- [1] Wildi, F., Bouchy, F., Doyon, R., Artigau, É., Blind, N., Reshetov, V., Hernandez, O., Blind, N., Genolet, L., Thibaut, S., Brousseau, D., Delabre, B., "NIRPS: an adaptive-optics assisted radial velocity spectrograph to chase exoplanets around M-stars" Tech. and Inst. for Det. of Exoplanets SPIE VIII, 10400-10441 (2017).
- [2] Yan, J., Asami, T., Harada, H., Kuriyagawa, T., "Fundamental investigation of subsurface damage in single crystalline silicon caused by diamond machining", *Prec. Eng.* 33, 378-386 (2009).
- [3] Yin, J., Bai, Q., Li, Y., Zhang, B., "Formation of subsurface cracks in silicon wafers by grinding" *Nanotech. and Prec. Eng.* 1, 172-179 (2018).
- [4] Trost, M., Herffurth, T., Schmitz, D., Schröder, S., Duparré, A., Tünnermann, A., "Evaluation of subsurface damage by light scattering techniques," *Appl. Opt.* 52, 6579-6588 (2013)
- [5] Zarudi I., Zhang L., "Subsurface damage in single-crystal silicon due to grinding and polishing" *J. Mater. Sci. Lett.* 15, 586–587 (1996).